Seismic assessment of the medieval Armenian church in Famagusta, Cyprus

Andrés Burgos Braga[1], Paulo B. Lourenço[2], Nuno Mendes[3]

[1]Formerly, Dept. of Civil Engineering, ISISE, University of Minho, Guimarães, Portugal,
andres.burgos.braga@gmail.com
[2]Dept. of Civil Engineering, ISISE, University of Minho, Guimarães, Portugal, pbl@civil.uminho.pt
[3]ISISE, University of Minho, Guimarães, Portugal, nunomendes@civil.uminho.pt

Abstract

This paper presents the analysis of the structural performance of the Armenian Church in Famagusta, Cyprus. Visual and photographic survey, non-destructive testing and numerical evaluation, using a tridimensional finite element model, are included. The non-linear behavior is analyzed under gravity and seismic loading, and pushover and time-history analysis are performed, including in both cases bidirectional loading. Results are studied in terms of capacity curves and damage patterns. The influence of the Church mass-distribution is also evaluated. As a result, the analysis estimates an adequate safety level of the building and various real damage features of the Church are justified and attributed to seismic actions.

Keywords: Medieval church; masonry; in-situ evaluation; seismic assessment; pushover analysis; non-linear time-history analysis.

1. Introduction

The walled city of Famagusta, located in the northeastern part of Cyprus (Figure 1a), was once one of the richest cities in the world thanks to its key location on the Eastern Mediterranean. Nonetheless, a long succession of invasions and several cycles of destruction and reconstruction of the city, led Famagusta to its inevitable decline. Today, the Cypriot port is politically within the self-proclaimed Turkish Republic of Northern Cyprus and is an embargoed and internationally isolated region, threatened by earthquakes, abandonment and neglect. Due to the severe state of deterioration of its vast architectural richness, the port city was placed on the 2008 World Monuments Watch List of 100 Most Endangered Sites by the World Monument Fund [World Monuments Watch, 2008].

One of the biggest latent threats affecting the built cultural heritage of Famagusta comes from the seismicity of the region. According to the Unit of Environmental Studies of Cyprus [2004], the island is situated within the second most intensive seismic zone of the earth – the Alpine-Himalayan belt; and its seismicity is attributed to the subduction of the African Plate under the Eurasian Plate, forming the denominated "Cyprus Arc".

Cyprus was struck by several earthquakes in the past. Between 26 B.C. and 1900 A.D., sixteen earthquakes occurred with intensities of VIII, or higher, on modified Mercalli scale. After 1896, more accurate data started to be collected and, since then, more than 400 earthquakes had epicenters on Cyprus and its surroundings. Two strong events damaged Famagusta, in 1924 and 1941, with magnitudes of about 6.0 [Unit of Environmental Studies, 2004]. According to the Seismic Hazard Map of Cyprus

(Figure 1b) (return period: 475 years), the design ground acceleration on rock for Famagusta is 0.25g (where g expresses gravity acceleration), which is the highest value within the whole territory. The city is located over loose terrace deposits, mainly formed by calcarenites, sands and gravels, which are likely to increase the hazard. A soil factor S equal to 1.35 (type "D") is recommended, leading to a PGA of 0.34 g [Safkan, 2012].

The present study focuses on the condition and structural behavior of the Medieval Armenian Church in Famagusta, which is valuable because of its still surviving, but highly damaged, fresco paintings. Various features needed in a conservation project are addressed here, including historical photographic survey, visual inspection and non-destructive in-situ tests. Particularly, dynamic identification and sonic testing were carried out to characterize the masonry present condition and the dynamic properties of the building. Additionally, the old and present damage of the Church and its safety are assessed based on a tridimensional finite element model, which is used for analyzing the non-linear behavior of the structure under gravity and seismic loading. The seismic performance of the building is studied by means of non-linear static pushover analysis and non-linear time-history analysis.

It is noted that few built cultural heritage buildings in Famagusta have been studied before, given the difficult political situation, and that the present building is abandoned but not in ruined condition. A seismic assessment of other churches in the city can be found, e.g., in Lourenço *et al*. [2012] for abandoned ruins and Votsis *et al*. [2015] for an in use cathedral, where also finite element modelling and non-destructives tests were performed. Other studies with similar procedures to the present research, which were successfully applied to complex masonry buildings, can be found, e.g., in Mendes *et al*. [2010], Marques *et al*. [2013], Roca *et al*. [2013] or Milani and Valente [2019]. Still, the combination of *in situ* testing with the use of static and dynamic analyses, as done in this paper, remains then subject of a very limited number of papers, given the required resources and computational demand. Moreover, the consideration of bidirectional loading in static analyses, as done here, is also uncommon.
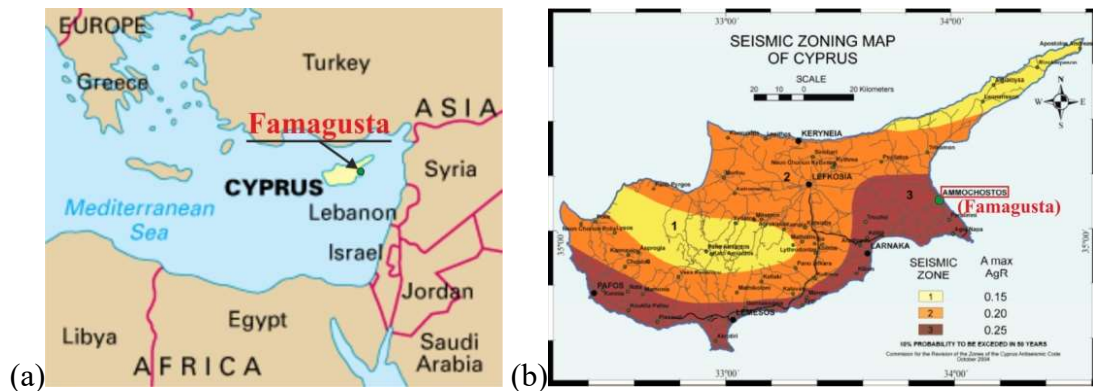

FIGURE 1: Cyprus and the city of Famagusta. (a) Location of Famagusta; and (b) Seismic Hazard Map of Cyprus [CYS EN 1998-1:2004, 2010] (Return period: 475 years).

2. The Armenian Church: Historical survey and visual inspection

The Armenian Church lies inside the fortified historic zone of Famagusta, in what used to be the city's Syrian quarter. Its original name and date of construction are unclear. Based on historic records, it could have been part of a monastery; and it might have been

built during the 14th century as a memorial of Armenian war refugees in Famagusta [Langdale *et al.*, 2009].

The Church is made of limestone ashlar masonry and is architecturally simple. The interior consists of a one-bay rectangular nave that ends at the east with a double-arch leading to a semicircular, pointed semi-domed apse (Figure 2a). The nave is covered by a groined vault of stone, with short barrel vaults to east and west. Doors are present on the west, south and north walls (the latter presently closed with brick masonry), and single windows are found on each side of the building. Moreover, the interior of the Church is decorated with three niches as well as with remnants of fresco paintings that, currently, are in an advanced state of deterioration. Many of the frescoes have been whitewashed over, with only the upper registers still visible [Langdale *et al.*, 2009].

The exterior of the Church (Figure 2b) bears few architectural articulations with no sign of sculptures. The sides are crowned with gables and only the upper section on the west façade is flattened so as to support a now lost belfry. In addition, the top of the north and south portals are characterized by lintels with relieving arches above. The dimensions of the Church, as shown in Figure 3, are about 6.7 m wide, 11.5 m long and 8.9 m high; the apse has a radius of 1.7 m; and the wall thickness is 0.7 m. The building is roughly symmetrical in its longitudinal east-west axis. Note that, in Figure 3, the dashed lines show the shape of the crossed-vault and of the internal double-arch that leads to the apse. Openings are marked with shaded areas.
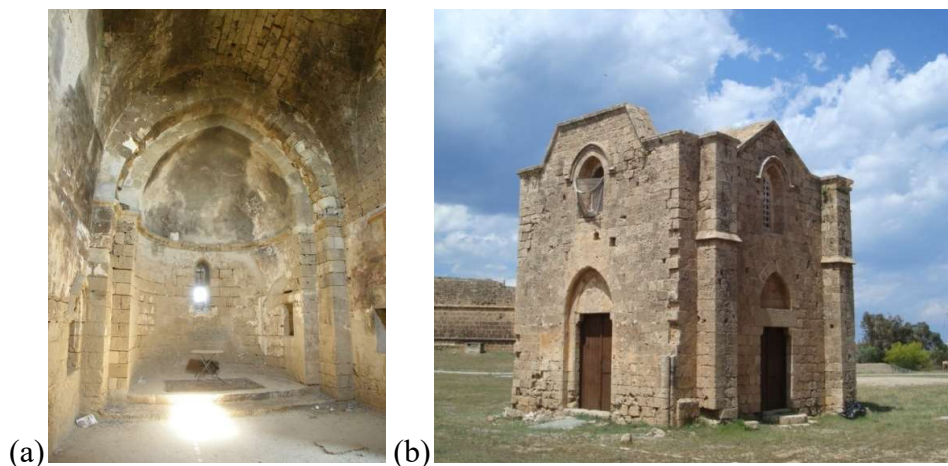

(a)　　　　　　　　　　　　(b)

FIGURE 2: Interior and exterior features of the Armenian Church. (a) East-end of the Church viewed from the interior; and (b) the Church exterior view from the southwest.

The Church might have notably deteriorated from mid- to late 19th century. Figure 4a presents a drawing of the Armenian Church, made in 1862, where it shows a general good condition except for some blocks that had fallen away from around the south portal and some visible loss of material on the northwest and southeast top corners. The same drawing also shows the still surviving belfry at the top of the west gable. In comparison, Figure 4b presents another drawing of the Church, made in 1896, from the same angle. Here, the failure of the south portal is visible and the partial ruin of the vaulting at the western and southern tips of the gables is suggested. The bell tower is lost as well as part of the west window; and the loss of material seems to have notably increased. No strong earthquake seems to have been reported within this period.

In 1878, the British took control of the port city and started restoration works in various Famagusta's monuments, including the Armenian Church. Figure 5 shows the state of the

building in 1911, after some stabilization works, which can be distinguished by the light-colored stone. Note that the gable of the west façade has fallen and damage has affected part of the dome and east wall. Also, the partial collapse of the masonry around the north entrance, including the lintel, is suggested. Moreover, these pictures show part of a small sacristy that used to be attached to the apse but is now no longer existent.
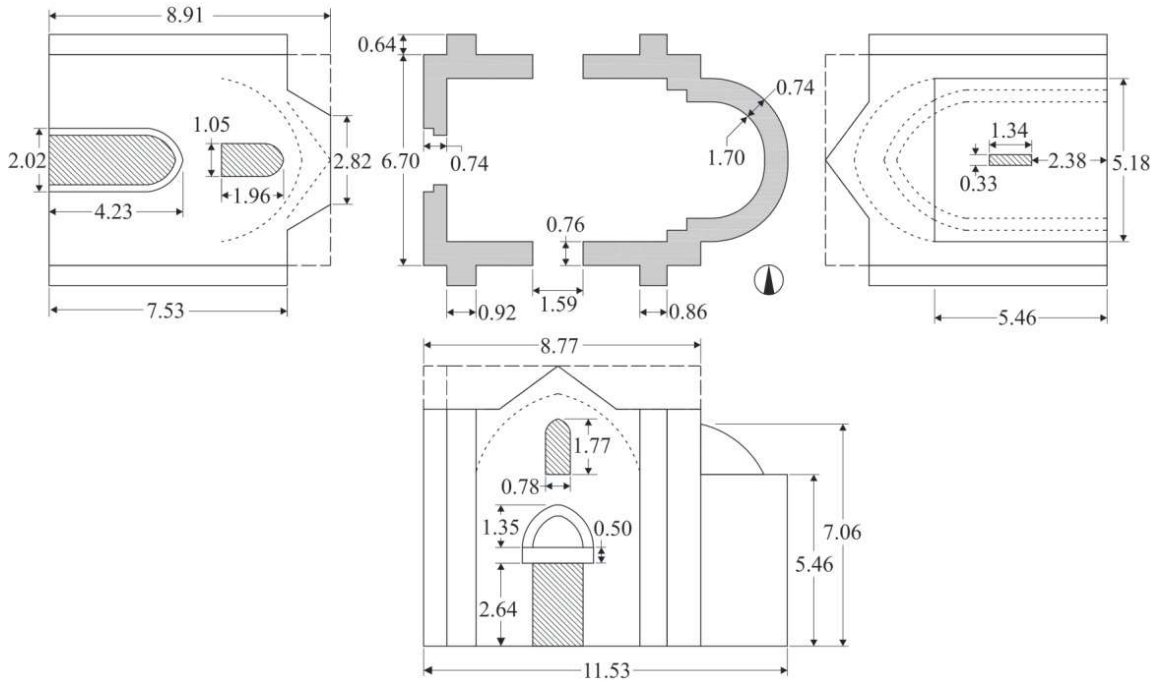

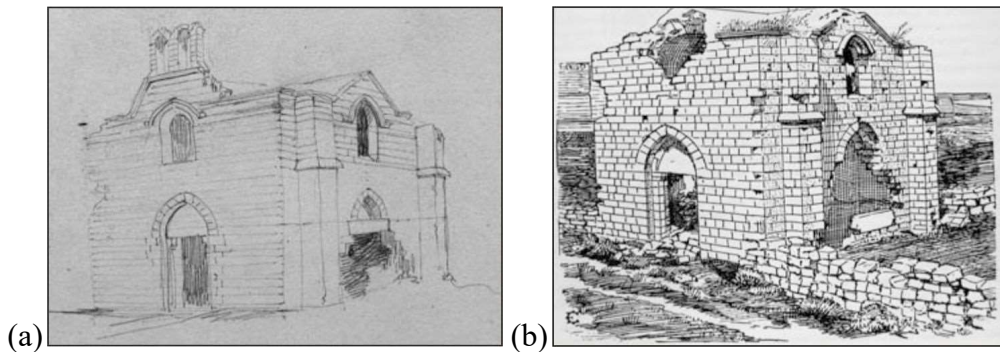
FIGURE 3: Geometry of the Armenian Church. Units: m.

FIGURE 4: The Church on the 19th century. (a) Drawing by E. Duthoit, pencil on paper, 1862 (Museum of Picardie, Amiens); and (b) drawing by C. Enlart, 1896 from [Enlart, 1899].

Subsequently, the most thorough restoration of the building happened from 1937 to 1945. The roof, and the north and south portals were reconstructed and consolidated; the lost and deteriorated masonry was rebuilt and replaced; and the north entrance was definitively closed with brick masonry. Note that the last strong earthquake that affected the city occurred in 1941, some years before the works were finished.

From 1945 to nowadays, the condition of the building seems not to differ much as shown in Figure 6. The exterior of the Church is today characterized by (Figure 7): (a) cracks between openings and above the dome; (b) stone deterioration mostly at bottom

4

sections, probably due to splashing rain and rising damp; (c) loose stone units that need to be consolidated; (d) biological activity, namely vegetation at base and roof level; (e) windows without proper protection against environmental elements; (f) inefficient buttressing due to material loss; (g) deteriorated mortar joints in various areas; and (h) presence of cavities in the walls, some of which are not original and need to be filled in. Regarding the roof and dome, due to the presence of plaster, no important cracks are visible; only vegetation and lichens are present.

Likewise, the interior of the Church is mostly distinguished by deteriorated stone and mortar joints. In particular, the vault is in bad condition, which can be caused by the inefficient protection against water infiltration (Figure 8a). Moreover, similar to the external cracks, the internal cracks are mainly located between openings at the north, south and west walls; and also at the top of the double-arch that leads to the apse (Figure 8b). Other cracks may also be hidden under the plaster that covers most of the bottom-half section of the walls.
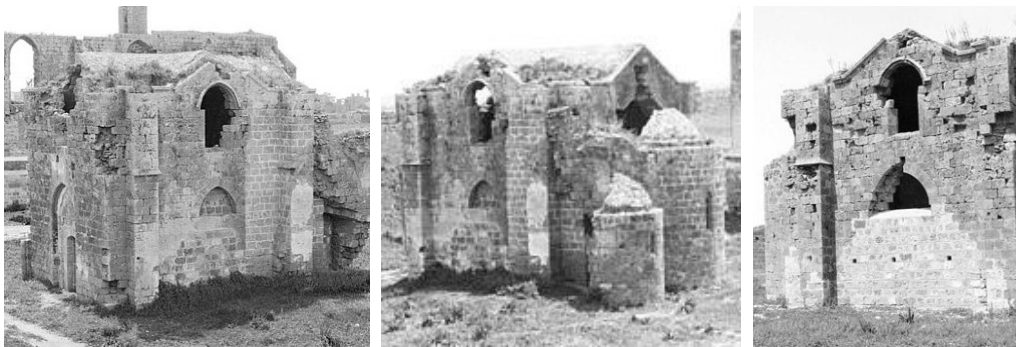

FIGURE 5: The Church in 1911 (Médiathèque de l'architecture et du patrimoine, France).
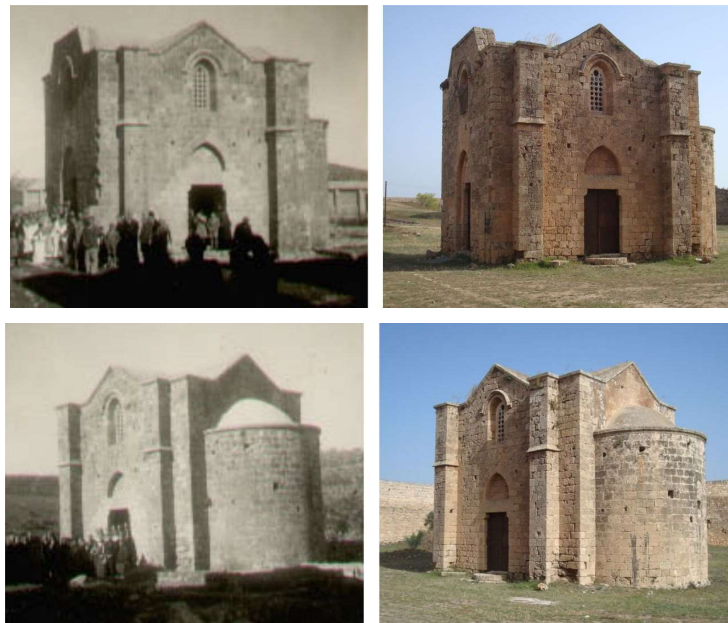

FIGURE 6: Visual comparison of the state of the Church: 1945 situation vs. present condition (Historical pictures from the Mogabgab Archive, Famagusta).
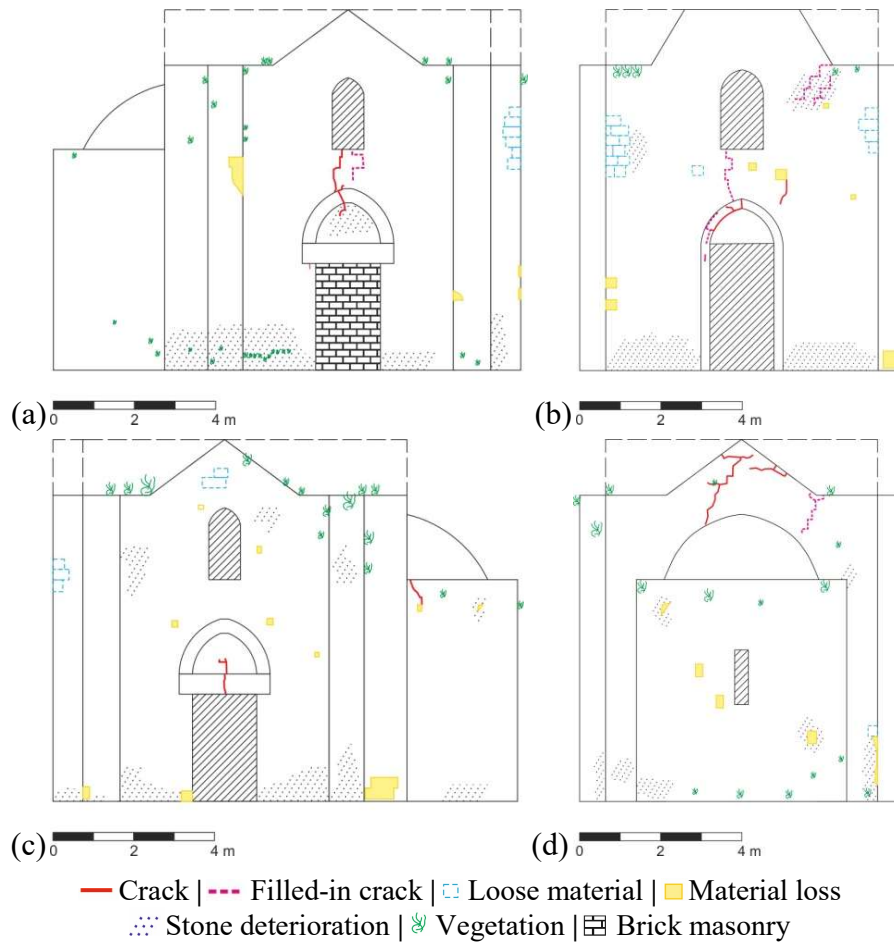
FIGURE 7: External damage maps of the: (a) north, (b) west, (c) south and (d) east sides of the Armenian Church.
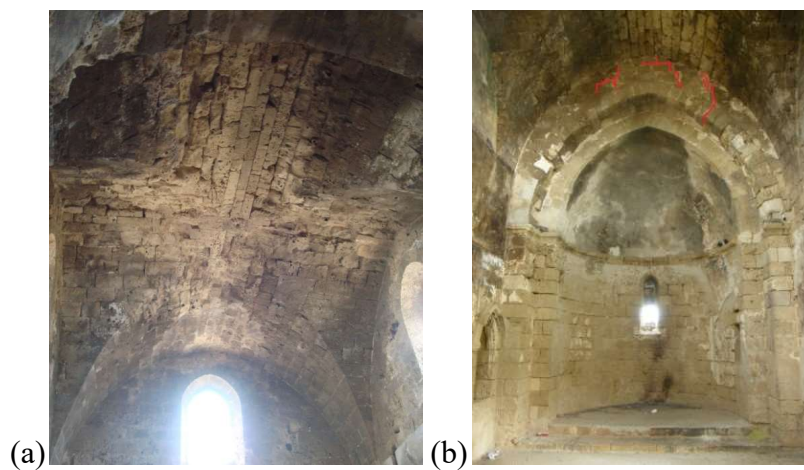

FIGURE 8: Deteriorated state of (a) the vaulted roof and of (b) the internal double-arch (with highlighted cracks at the top).

3. In-situ testing

3.1 Dynamic identification test

Dynamic identification combines vibration testing techniques and analytical methods to determine modal parameters of structures, i.e. frequencies, mode shapes and damping coefficients. These parameters are essential to understand how a structure responds statically to different loads or dynamically to vibratory events; and can be used to calibrate the numerical model of a structure [Lourenço *et al.*, 2012]. In detail, the shape of the vibrations modes allows to detect damage and inadequate connections between structural parts, while the frequencies allow obtaining the Young's modulus of the material(s) in the structure. This is further corroborated by the comparison between the measured dynamic response and the simulated response in a computer, which truly validates the quality of the numerical model. Only after validation, should a model be used for safety predictions. With this purpose, the Armenian Church was excited with ambient vibrations and output-only modal identification techniques were applied. Four piezoelectric accelerometers (sensitivity equal to 10 V/g, frequency range from 0.15 to 1000 Hz, dynamic range ± 0.5g) were used to measure the accelerations. The sensors were connected to a laptop by a data acquisition system (DAQ) with 24-bit resolution using USB cable connection. Long periods of measurements were recorded (15 minutes) with a sampling rate of 200 Hz and the signal was processed using Stochastic Subspace Identification methods by means of the software ARTeMIS Modal Pro [ARTeMIS, 2018]. During the measurement periods, the ambient temperature was recorded but variations were negligible.

Six setups were performed using two reference sensors, positioned at roof level, and moving another two around the structure, i.e. over the roof, windows and apse. Figure 9a illustrates one of the setup configurations with the reference (*R*) and free (*F*) sensors placed on the west top corners of the Church. Here, the arrows indicate the direction of the measured acceleration. Moreover, Figure 9b shows some views of the dynamic measurements where the sensors were positioned with the aid of an elevating work platform. In total, the first six modes of vibration of the Church were identified. Table 1 presents the estimated frequencies and damping ratios of the six modes, as well as the standard deviation of these parameters.

TABLE 1: Estimated frequencies and damping ratios (SSI-UPC method was used).

Mode	Frequency [Hz]	Frequency standard deviation [Hz]	Damping ratio [%]	Damping ratio standard deviation [%]
1	5.66	0.03	0.93	0.14
2	8.72	0.04	2.25	0.30
3	10.84	0.08	0.88	0.13
4	12.56	0.14	1.33	0.53
5	15.97	0.12	1.00	0.16
6	16.43	0.12	1.12	0.31

In general, the first modes of a civil engineering structure present the higher contributions for its global dynamic behavior. In these cases, the first modes can be

assumed as enough for the characterization of the dynamic properties [Lourenço *et al.*, 2012]. Furthermore, a high number of modes could lead to difficulties in the calibration of the numerical model. Here, the six identified frequencies ranged from 5.7 to 16.4 Hz, with well-spaced values, except for the fifth and sixth modes that are rather close. Concerning the damping ratios, a significant variation was observed with an average value of 1.25%. The average standard deviation of the frequencies is low. However, the damping ratios present some significant standard deviations. It is noted the damping ratio is a very sensitive parameter and difficult to estimate from experimental tests [Mendes, 2012], mainly when ambient vibration is adopted for excitation source. Regarding the mode shapes, shown in Figure 10, the first three deflected configurations are characterized by a global behavior of the structure, i.e. transversal, longitudinal and torsional; while the next three are mainly defined by the local deflection of the north, south and west facades.
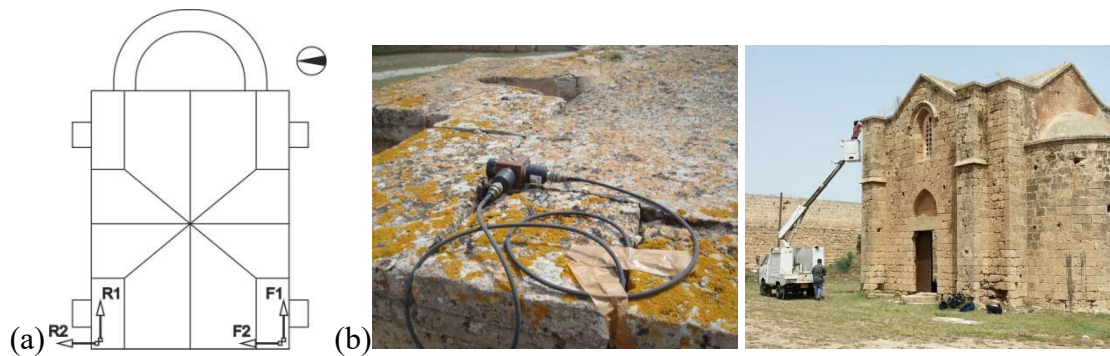

FIGURE 9: Dynamic identification. (a) One of the test setups showing the position of the reference (*R*) and free (*F*) accelerometers; and (b) views of the dynamic measurements.
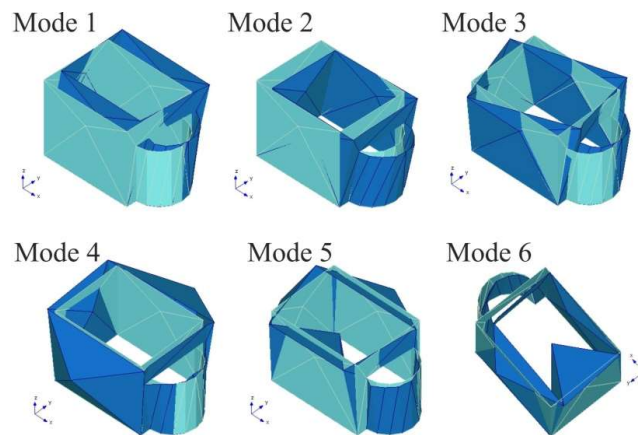

FIGURE 10: Experimental mode shape configurations identified by means of the software ARTeMIS Modal Pro.

3.2 Sonic testing

Sonic tests are based on the generation of elastic waves by sonic impulses at specific points of the structure. The travel time that the impulse takes to cover a known distance is measured with sensors, allowing the calculation of the sonic velocity through the medium. This technique is useful to qualitatively assess the structural morphology by

correlating the results with other non-destructive tests, and to detect voids and cracks, among others [Binda *et al.*, 2001]. Sonic testing can also be used for the mechanical characterization of masonry, because the velocity of an elastic wave passing through a solid material depends on its density (ρ), dynamic modulus of elasticity (E_d) and Poisson's ratio (v). In reality, masonry can be very inhomogeneous; hence, obtained values can be indicative. The estimation of E_d can be done by measuring the velocity of propagation of the elastic compression (V_P) and Rayleigh surface (V_R) waves; based on Equations 1 and 2, respectively.

$$V_P = \sqrt{\frac{E_d(1-v)}{\rho(1+v)(1-2v)}} \qquad (1)$$

$$V_R = \frac{0.87+1.12v}{1+v} \cdot \sqrt{\frac{E_d}{\rho} \cdot \frac{1}{2(1+v)}} \qquad (2)$$

Two configurations of sonic tests were performed to the Armenian Church: direct and indirect testing. In both cases, the impulse was induced with a hammer hit next to one accelerometer (transmission sensor), while the other accelerometers (receivers) were placed at known distances. The sensors were connected to a laptop using a DAQ with 24-bit resolution and a sampling rate of 25 kHz.

Direct testing was performed in two locations of the Church – the south wall and the southwest buttress. The purpose was to evaluate the masonry condition and, in particular, to assess the presence of internal voids, different materials or if repair works had occurred there. On each location, two vertical columns (A and B) and four horizontal levels were tested (4 pairs of points per column).

Regarding the south wall (Figure 11a), the sonic velocity ranged from 1170 to 2140 m/s and the average values in A and B were 1810 and 1550 m/s, respectively. In general, Column A presented higher values with low variation, indicating that the masonry around the entrance was probably rebuilt with new stone units in the past; while most of the stones located afar may still be the original ones in worse condition. Concerning the buttress (Figure 11b), the sonic velocity ranged from 1240 to 2260 m/s and the average values in A and B were 1360 and 1920 m/s. The outer masonry layer (column B) showed a better condition than the internal section, indicating that the outer stone units might have also been replaced in the past or some weak filling / voids are present inside the buttress. In both tests, the coefficient of variation was lower than 10%.

The indirect test configuration was adopted on the north wall, next to the entrance, with the aim of estimating the dynamic modulus of elasticity of the Church's masonry. The test was performed along two columns, with four levels each. The impulses were generated, per column, at the bottom level; while the sensors positioned at levels 2 to 4 (each one separated by 0.5 m) measured the travel time of the P and R-waves. The testing grid was designed so that the measuring points were separated by at least one mortar joint. The average values of the P and R-wave velocities were 1480 and 606 m/s, respectively; and the calculated dynamic modulus was 1880 N/mm^2, using an estimated unit weight of masonry of 1.6x10^{-5} N/mm^3.
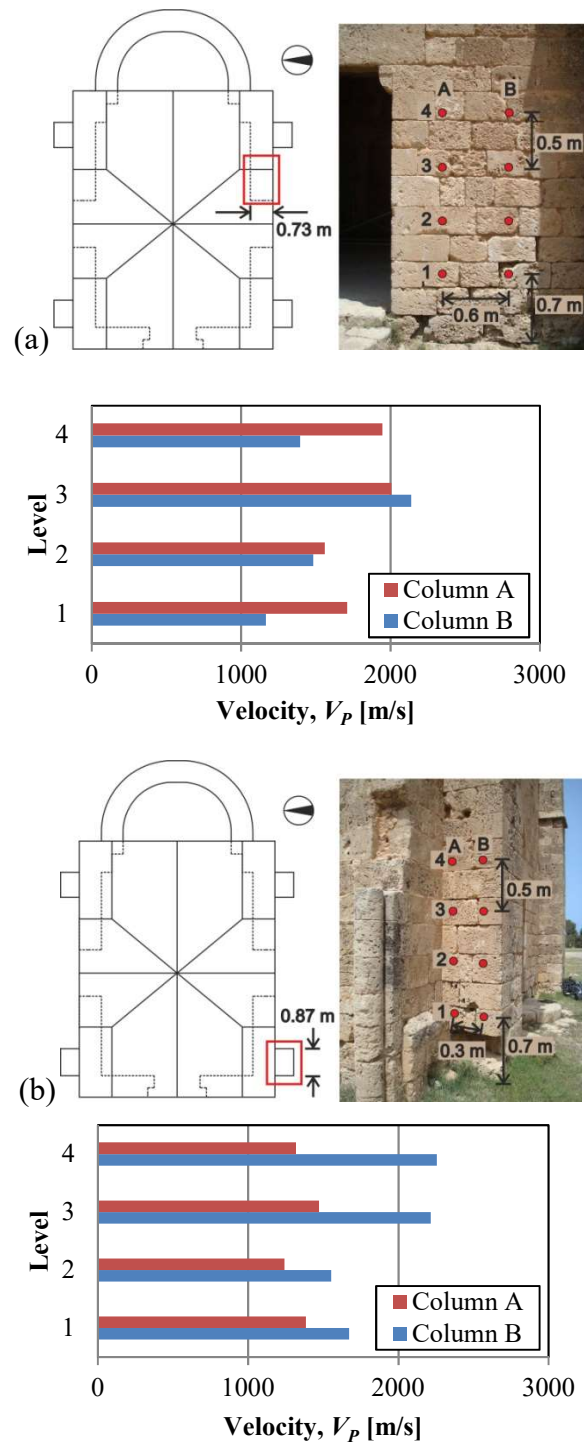
FIGURE 11: Direct testing locations, grids and measured velocities of the (a) south wall and (b) southwest buttress.

4. Numerical model and model updating

4.1 Definition of the numerical model

The numerical model of the Armenian Church was built using the finite element software DIANA [DIANA FEA BV, 2018] with the aid of geometrical data gathered from

available laser scanning. A macro-modeling approach for masonry was adopted, and a tridimensional model was developed considering the relatively simple geometry of the Church. The generated finite element mesh, shown in Figure 12, is composed of two types of regular solid elements: twenty-node isoparametric solid brick elements and fifteen-node isoparametric solid wedge elements. This last type of element corresponds to less than 1% of the whole model. In total, the model is formed by 10,448 elements with 53,309 nodes and 159,927 degrees of freedom. Regarding the boundary conditions, all degrees of freedom of nodes at ground level ($Z = 0$) were restricted.

The physical non-linear behavior of masonry was simulated using a Total Strain Crack Model (TSCM), while a Rotating Crack Model, or coaxial stress-strain concept, was adopted to control the crack-opening direction [DIANA FEA BV, 2018]. The TSCM is an isotropic model with a compressive cap and a smeared approach for the fracture energy, and it was selected because it provides good stability in the crack-opening control at a moderate computational cost [Lourenço et al., 2012]. As shown in Figure 13 (not drawn to scale), the tensile masonry behavior was defined using a post-peak exponential softening, whereas parabolic hardening, followed by post-peak parabolic softening, was chosen for compression. Furthermore, in order to ensure mesh independency of the solution, both tensile (G_f^I) and compressive (G_c) fracture energies were regularized taking into account the finite element size, using a regularization length (h) equal to the cubic root of the volume of the element.
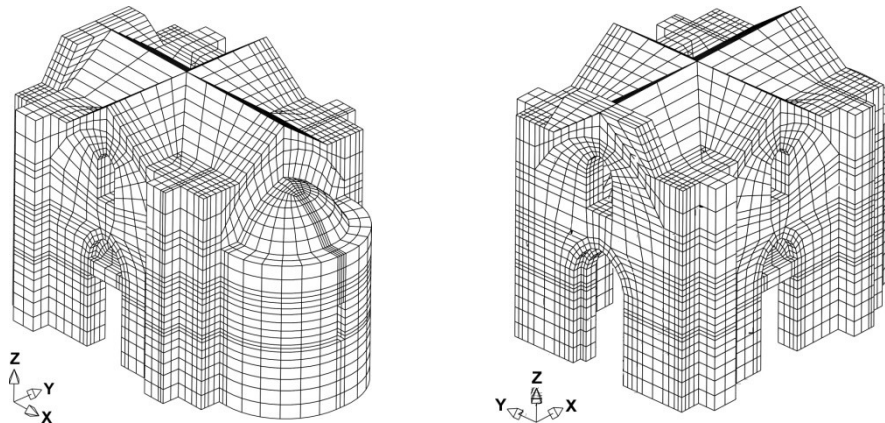

FIGURE 12: Views of the finite element mesh of the Church.

Table 2 presents the physical and mechanical properties of masonry that were adopted based on literature [Lourenço, 2010] and on the previous study of another Famagusta building [Lourenço et al., 2012]. A relation $E = \alpha \cdot f_c$ was used, with α equal to 500. As noted by Lourenço et al. [2012], the parameter α is rather variable for masonry with values ranging from 200 to 1000. Moreover, the ductility index for compression was taken equal to 1.6 mm, which is a suggested value for a compressive strength lower than 12 N/mm^2. The ductility index for compression corresponds to the ratio G_c/f_c, which represents the fracture energy normalized by the compressive strength (f_c) [Chiaia et al., 1998], [Vasconcelos, 2005]. The masonry tensile strength and the tensile fracture energy were assumed equal to 0.2 N/mm^2 and 0.02 N/mm, respectively. These values describe a very low strength material, yielding finally a zero strength response.

TABLE 2: Linear-elastic and non-linear masonry properties.

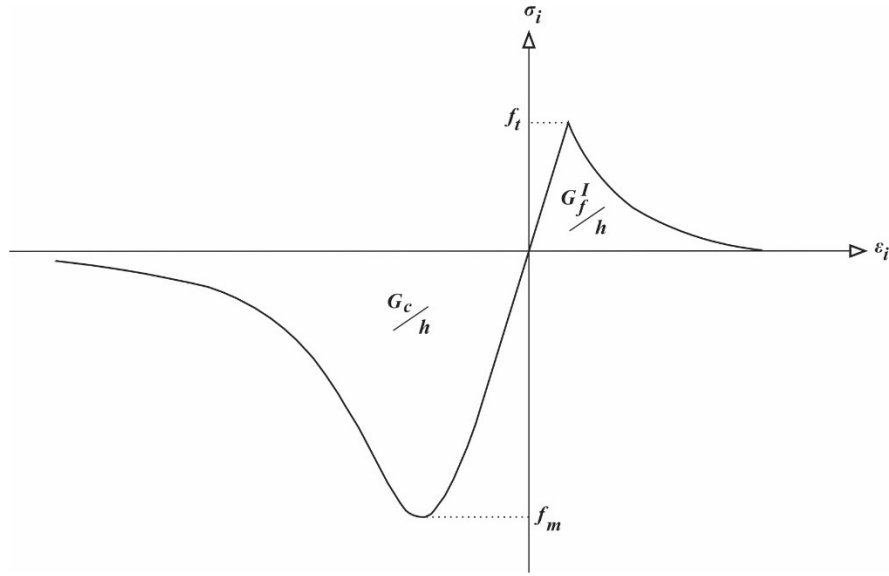| Material property	Symbol	Unit	Value
Unit weight of masonry	γ	N/mm^3	1.6x10^{-5}
Modulus of elasticity	E	N/mm^2	1100
Poisson's ratio	υ	----	0.2
Ductility index in compression	$d_{u,c}$	mm	1.6
Masonry compressive strength	f_c	N/mm^2	2.2
Compressive fracture energy	G_c	N/mm	3.5
Masonry tensile strength	f_t	N/mm^2	0.2
Tensile fracture energy	G_f^I	N/mm	0.02

FIGURE 13: Adopted inelastic behavior of masonry (not drawn to scale).

4.2 Numerical model updating

The updating of the numerical model was accomplished by means of Modal Response analysis. Initially, the first six numerical modes of vibration were calculated (Figure 14), using the adopted material properties of Table 2, and compared to the experimental results of the dynamic identification. Table 3 presents the percentage of error of the estimated numerical frequencies (f_{NUM}) with respect to the experimental ones (f_{EXP}), which serve as a reference. Also, the mode shapes are compared in terms of the Modal Assurance Criterion (MAC) according to Equation 3, where $\{\varphi_{NUM}\}$ and $\{\varphi_{EXP}\}$ are the numerical and experimental eigenvectors, and the variables r and q go from 1 to 6, representing the compared modes. Note that the result of this equation is bounded between 0 and 1, with 1 expressing fully consistent mode shapes.

$$MAC\ (r,q) = \frac{|\{\varphi_{NUM}\}_r^T\{\varphi_{EXP}\}_q|^2}{(\{\varphi_{NUM}\}_r^T\{\varphi_{NUM}\}_r)(\{\varphi_{EXP}\}_q^T\{\varphi_{EXP}\}_q)} \tag{3}$$

From Table 3, it can be seen that the maximum error is lower than 5% for all the modes, with an average error of 2.7%. Moreover, the MAC values emphasize a good

12

consistency of the first four deflected configurations (average of 0.89). In particular, modes 1 and 2, which possess 73% and 76% of the total mass participation in the transversal (Y) and longitudinal (X) directions, respectively, presented a virtual flawless consistency. This outcome denotes a good agreement between the numerical and real geometrical features of the Church.
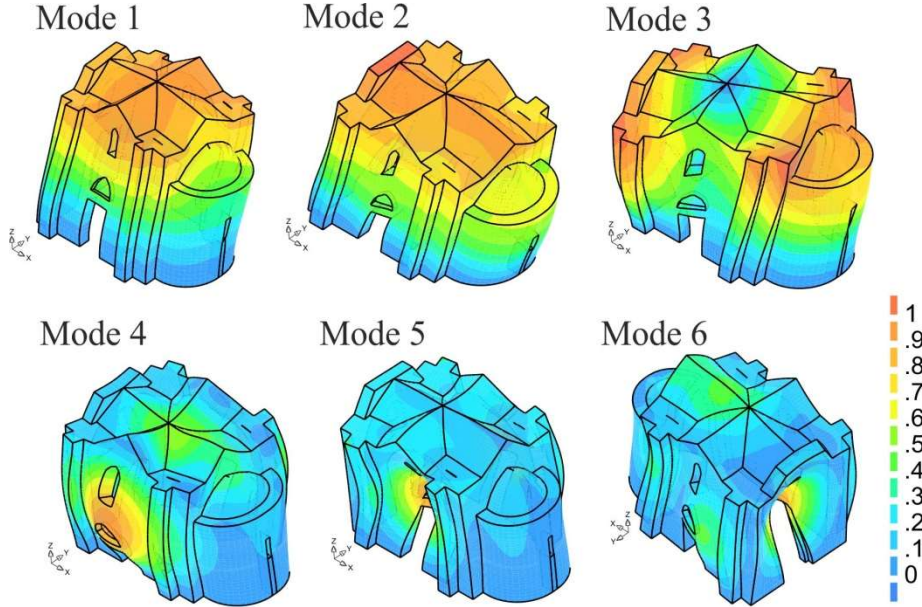

FIGURE 14: Numerical mode shape configurations (deformation scaled to a unitary value).

By comparing the modulus of elasticity obtained for the global model, i.e. 1100 N/mm² (refer to Table 2), with respect to the dynamic modulus of elasticity calculated from sonic testing (i.e. 1878 N/mm², as reported in Section 3.2), a low ratio of 0.60 is obtained. In literature, various formulas exist to correlate the moduli of concrete structures; one simple empirical relation offers a ratio of 0.83 between them [Lydon *et al.*, 1986]. Here, it is noted that the difference between these values is not so large, given that one measurement is local (sonic testing) and the other is global (dynamic identification). The walls of the building are multiple leaves and some damage is visible, which justify an elasticity modulus for the structure lower than the one measured in relatively solid stone masonry. Consequently, a masonry modulus of elasticity of 1100 N/mm² is adopted in the following.

TABLE 3: Comparison of experimental and numerical frequencies and mode shapes of the numerical model.

Mode	f_{EXP} [Hz]	f_{NUM} [Hz]	Error [%]	MAC
1	5.66	5.72	1.06	1.00
2	8.72	8.98	2.98	0.99
3	10.84	10.96	1.11	0.98
4	12.56	12.08	–3.82	0.94
5	15.97	15.25	–4.51	0.61
6	16.43	16.89	2.80	0.79
		|Average|	2.71	0.89

5. Non-linear safety analysis

To understand the current damage of the Armenian Church and to assess its structural behavior, non-linear analyses were first performed for vertical and horizontal loading following a mass-proportional load-pattern approach, independently from their height distribution in the structure, since good correlations have been found in terms of capacity between mass proportional pushover analysis and time history analysis in previous studies performed on historical constructions [Endo *et al.*, 2017], [Peña *et al.*, 2010].

The full Newton-Raphson method, based on an energy convergence control with tolerance 10^{-3}, was adopted for solving the non-linear problems arising from the equilibrium and compatibility conditions. Moreover, the line-search algorithm and arc-length control were also used. The former helps stabilizing the convergence rate by automatically scaling the incremental displacements in the iteration process; while the latter is used to determine the softening behavior of the load-displacement relation of the structure and to overcome the problem of predicting a large displacement for a given force increment and of following the post-peak response of a structure [DIANA FEA BV, 2018].

5.1 Vertical loading

Initially, only the self-weight of the structure was considered and the stress level was evaluated. Figure 15 presents the deformed shape and distribution of principal stresses of the structure under working stresses. The highest compressive stresses (Figure 15a) are located at the base, in the center of the vault and at the top of the dome. The maximum compressive stress is 0.34 N/mm^2, which is much lower than the compressive strength of the masonry (See Table 2). Moreover, the highest tensile stresses (Figure 15b) are located at the top of the windows, in the connection of the apse with the transversal east wall and at the top of the internal double-arch. The maximum tensile stress is 0.23 N/mm^2, which is in the range of the adopted tensile strength, indicating incipient cracking.

Next, the capacity of the building against vertical loading was analyzed by increasing gravity loads until failure. Figure 16a presents the force-vertical displacement diagram, indicating that the building was able to withstand approximately 6.5 times its own weight. An approximate linear behavior is observed until the structure reaches a ductile failure, which is corroborated by the final plateau of the curve. Note that the displacements were measured at the top of the internal double-arch, which was selected based on the response of the Church when subjected to its self-weight. In addition, Figure 16b shows the deformed shape and cracking of the building calculated at the beginning of the ductile behavior. Here, the cracking is measured by the maximum principal strain (ε_1), i.e. strain caused by pure tensile stresses. The failure mechanism of the Church corresponded to the localized failure of the apse side, whereas the rest of the structure shows an overall good condition, except for concentrated damage around the windows. These results indicate that the building presents a notable safety level in terms of vertical loading, which can be credited to the high stiffness, short spans and good load bearing capacity of the masonry walls in compression.
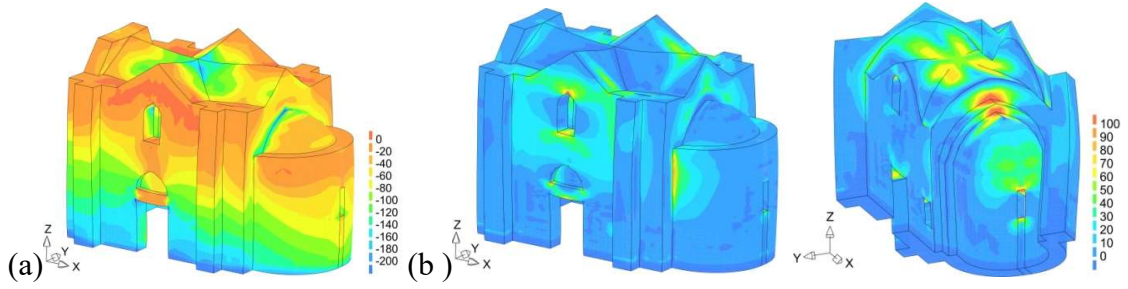
FIGURE 15: Deformed shape and distribution of (a) minimum (compressive) and (b) maximum (tensile) principal stresses, due to self-weight (in the last picture, the stresses are plotted on the internal surfaces of the vault and of north and east walls).
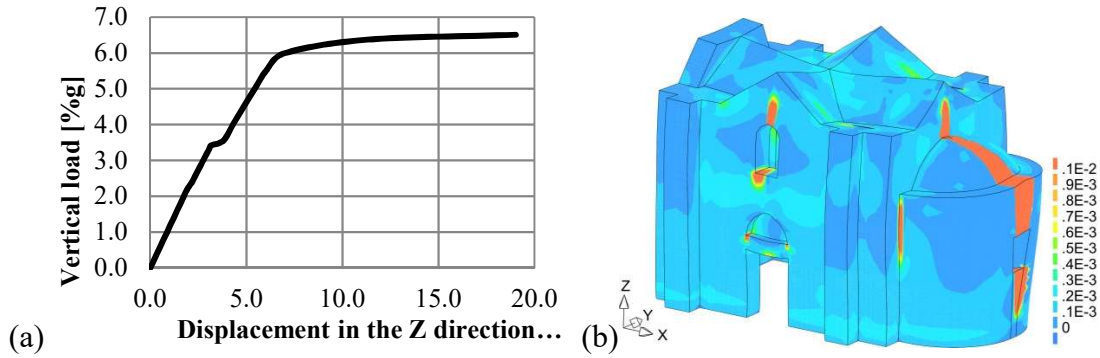

FIGURE 16: Capacity of the building against vertical loading. (a) Force-vertical displacement diagram, plotted at the top of the apse; and (b) deformed shape and cracking, given by the maximum principal strain ε_1, due to vertical loading, at maximum capacity.

5.2 Horizontal loading

The capacity of the Church against horizontal loading was evaluated by means of static pushover analysis. This is a method proposed by the Eurocode [EN 1998-1, 2004] to estimate the seismic response of a structure based on an incremental-iterative procedure under conditions of constant gravity loading and monotonically increasing horizontal loading. The structural performance is measured based on capacity curves, i.e. the seismic coefficient (α) vs. a given control displacement response, where the first term is defined as in Equation 4. Within this study, the pushover analysis was used, through the prediction of deformation and damage, to identify the weak features of the Church, to justify its old and current damage, and to assess its seismic safety condition.

$$\alpha = \frac{\sum Horizontal\ forces}{Self-weigh\ of\ the\ structure} \qquad (4)$$

To perform the analysis, two pushover loading patterns were applied: unidirectional and bidirectional mass-proportional. The first one is a uniform pattern based on lateral forces proportional to mass regardless of elevation. The second one considers the combination of two horizontal components acting simultaneously in principal orthogonal directions, X and Y. One direction follows a simple mass-proportional configuration, while, at the same time, 30% of the load is added to the other direction. Due to the irregularity of the building, these loading patterns were applied in both positive and

15

negative orientations of the global axes, representing the left-to-right and right-to-left seismic actions.

In total, eight mass-proportional pushover analyses were performed. Concerning the unidirectional loading pattern, four analyses were done, i.e. "+X", "−X", "+Y" and "−Y". Regarding the bidirectional loading pattern, taking into account the symmetrical behavior obtained in the Y direction from the previous load configuration, the positive and negative X global directions were combined with only one chosen Y orientation (the positive one), i.e."+X + 0.3 Y", "−X + 0.3 Y", "Y + 0.3 X" and "Y − 0.3 X".

5.2.1 Results

Figure 17 presents the resulted capacity curves, where the horizontal displacement of the structure was calculated based on the average displacement of the four top corners of the Church. Note that the "+Y", "Y + 0.3 X" and "Y − 0.3 X" capacity curves are superposed, slightly varying only on their post-peak behavior. Table 4 compares the maximum seismic coefficients.

TABLE 4: Comparison of the maximum unidirectional and bidirectional mass-proportional seismic coefficients α.

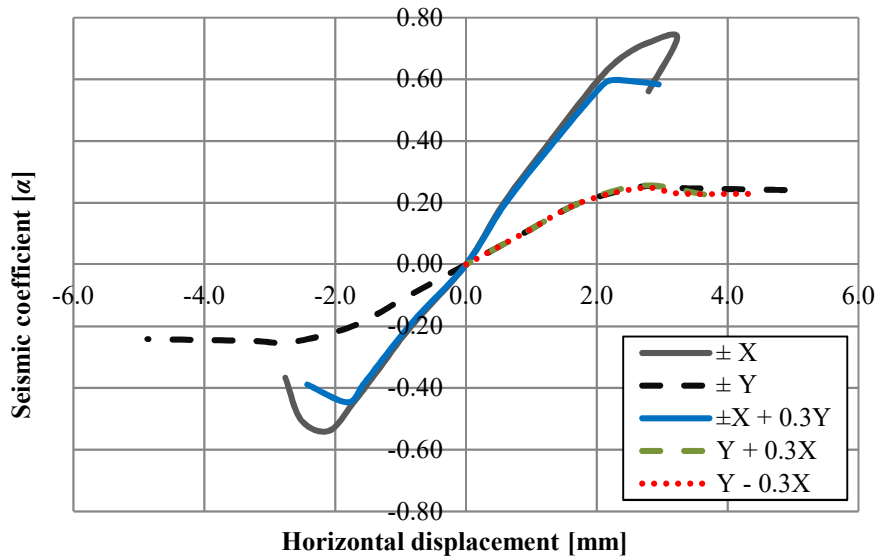| Unidirectional mass-proportional		Bidirectional mass-proportional		Difference [%]
Analysis	α	Analysis	α	
+X	0.74	(+X) + (0.3 Y)	0.60	19
−X	0.54	(−X) + (0.3 Y)	0.45	17
±Y	0.25	(±Y) + (±0.3 X)	0.25	0

FIGURE 17: Mass-proportional pushover capacity curves.
Bidirectional analyses: "±X", "±y" and "±X -0.3X".
Unidirectional analyses: "Y+0.3X" and "Y-0.3X". In these analyses, the loading was not applied in the negative Y direction.

From Figure 17, it is observed that the capacity of the Church is controlled by the transversal Y direction. The longitudinal X direction presents a better performance, which can be attributed to the sturdiness of the structure and the presence of the apse that limits the displacements. The failure mechanism of the structure in its transversal direction is characterized, to some extent, by a ductile behavior as demonstrated by the post-peak

tendency of the capacity curves. Contrarily, in its longitudinal direction, the structure is characterized by a quasi-brittle behavior. According to these curves, the building can withstand a transversal static horizontal acceleration of $0.25g$, which coincides with the PGA prescribed by the code for rock, but seems insufficient for the local soil conditions. Below, a time history analysis is carried out for validation.

Additionally, Figure 18 shows the cracking patterns of the building, given by the maximum principal strain. These patterns correspond to the analyses with the lowest seismic coefficients in both X and Y directions, which were measured at the end of the capacity curves, at failure. Damage is mainly concentrated between openings, which is a typical failure feature of masonry buildings; and is also present on the apse side and at the base; particularly at the corners of the entrances.
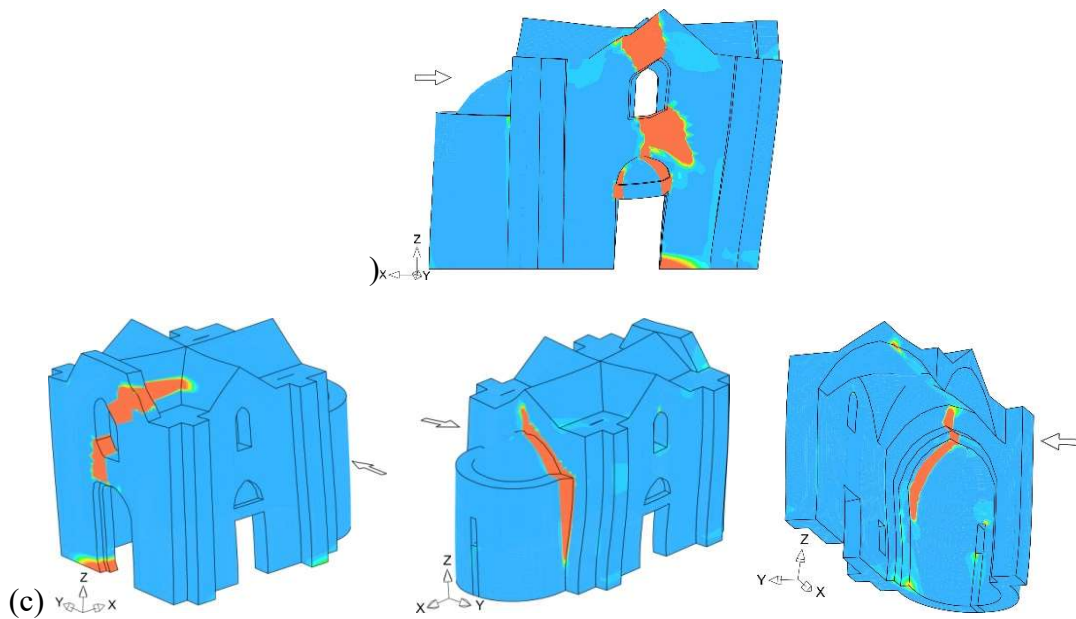

FIGURE 18: Deformed shape and cracking, given the maximum principal strain ε_1, based on pushover analysis. The results correspond to the following loading patterns: (a) "$(+X) + (0.3\,Y)$", (b) "$(-X) + (0.3\,Y)$", and (c) "$+Y$". The direction of the full mass-proportional load is given by the orientation of the white arrows, while the shaded arrows show the direction of the combined 30% loading.

6. Discussion on dynamic effects

With the aim of further analyzing the influence of the dynamic properties of the Church in its structural behavior and being able to thoroughly discuss about its safety condition, two additional approaches were taken into consideration. First, static pushover analysis based on a first-mode proportional loading pattern was used; and, afterwards, dynamic time-history analysis was performed.

6.1 Influence of mass distribution

The pushover analysis with a first-mode proportional loading pattern is another code-based procedure used to evaluate the structural seismic capacity. Within this "modal" pattern, the lateral forces are theoretically proportional to both mass and modal displacements, according to the fundamental mode shape in the direction under

consideration [EN 1998-1, 2004]. This might be unreasonable for historical masonry structures in the presence of modes that are not mostly translations and in the, usual case, of failure mechanisms involving large rigid macro-blocks, in which elastic dynamic characteristics play a limited role. For the "modal" pattern, lateral forces F_i, applied at every node i, are thus calculated as of Equation 5, where φ_i and φ_j are the modal displacements of masses m_i and m_j

$$F_i = \frac{\varphi_i \cdot m_i}{\sum \varphi_j \cdot m_j} \tag{5}$$

It is important to notice that the application of this procedure to complex finite element analyses can pose some difficulties, especially in determining the mass matrix of the numerical model. Here, two possible approximations of the code procedure are presented, where the applied lateral forces are proportional to modal displacements only. In the following, they will be referred to as pushover proportional to first-mode "V1" and "V2", detailed next. Note that these analyses were made considering only the most stringent behavior obtained from the mass-proportional pushover results, i.e. the one with the lowest safety factor $(+Y)$. Moreover, as mentioned before, in the transversal Y direction, it is precisely mode 1 the one that presents the highest mass contribution and it is therefore chosen as the fundamental mode shape in the analyzed direction.

Regarding the pushover proportional to first-mode "V1", the displacement pattern of mode 1 was first obtained via Modal Response analysis. The reaction forces at each node, which would produce the same deformed configuration in the structure, were then calculated through a linear-elastic analysis. These forces were subsequently applied to the model and monotonically increased until failure. This procedure has been used in the past for the study of historical buildings, e.g. Lourenço et al. [2012] and Mendes et al. [2010].

Alternatively, within the pushover proportional to first-mode "V2", the lateral forces F_i applied to the numerical model were calculated as of Equation 6 and, again, were increased until failure. Here, φ_i is the vector of modal displacements, and φ_T and m_T are constant values representing the sum of the modal displacements and the total mass of the building, respectively. This approximation of the code procedure corresponds to having the mass matrix equal to the identity matrix (lumped mass matrix).

$$F_i = \frac{\varphi_i}{\varphi_T \cdot m_T} \tag{6}$$

Figure 19 compares the resulted capacity curves measured through pushover proportional to first-mode "V1" and "V2", with respect to the mass-proportional capacity curve in the $+Y$ direction previously obtained (See Section 5.2). As observed in this graph, the capacity curve proportional to first-mode "V1" presents a totally different stiffness compared to the others. This approach was certainly not able to correctly reflect the mass-distribution of the building, changing the contribution of mode 1. Contrarily, the capacity curve proportional to first-mode "V2" presents a good approximation with respect to the mass-proportional approach. In this case, the maximum static horizontal force that the building can support is reduced by approximately 20%. Additionally, the resulting deformed shape and damage pattern is similar to the one obtained from the mass-proportional approach and, therefore, it is not repeated (See Figure 18c).
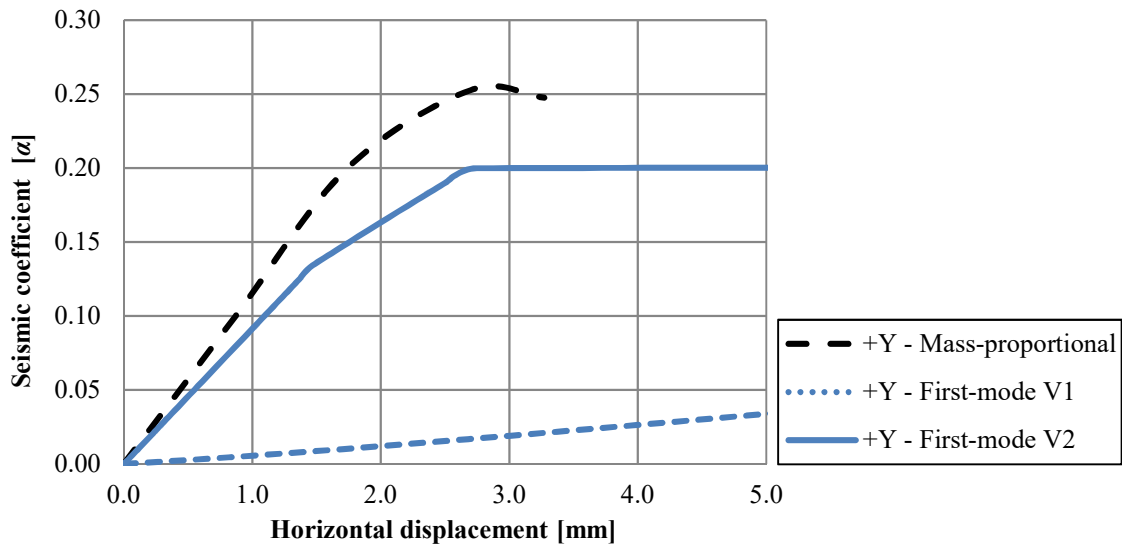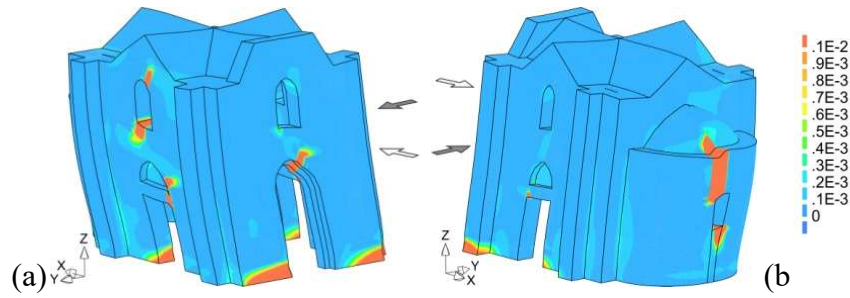
FIGURE 19: Comparison of capacity curves obtained with pushover proportional to first-mode "V1" and "V2" (blue color), with respect to the mass-proportional pushover capacity curve (black color) in the +*Y* direction.

6.2 Dynamic evaluation of the Church

The dynamic behavior of the Church was finally evaluated using time-history analysis. Within this method, the horizontal seismic action is described by two orthogonal and independent components, represented by the code response spectrum. Here, two uncorrelated artificial accelerograms, acting in directions X and Y of the numerical model, were built accounting for the "Type 1" elastic response spectrum defined by the Eurocode 8 [EN 1998-1, 2004] and the Cyprus National Annex [CYS EN 1998-1:2004, 2010]. The spectrum, which is shown in Figure 20, was defined with a damping ratio ξ of 5% and a ground type "D", according to the geological characteristics of Famagusta [Safkan, 2012]. The peak ground acceleration (PGA) is equal to 3.4 m/s^2, corresponding to the design ground acceleration on rock, affected by the ground factor. Additionally, Figure 21 presents the artificial accelerograms, which were generated by means of the software SIMQKE_GR [Gelfi, 2006] with a baseline correction filter using SeismoSignal [Seismosoft, 2018]. The total time of the seismic action was set equal to 20 s, including a duration of 10 s for the stationary part of the seismic action.

Note that, to assess the dynamic behavior of the Church, three earthquakes of different intensities were used. To this aim, the artificial accelerograms were affected by scaling factors (1.0, 2.0 and 4.0): (1) Earthquake 1: PGA$_1$ = 3.4 m/s^2; (2) Earthquake 2: PGA$_2$ = 6.8 m/s^2; (3) Earthquake 3: PGA$_3$ = 13.6 m/s^2.
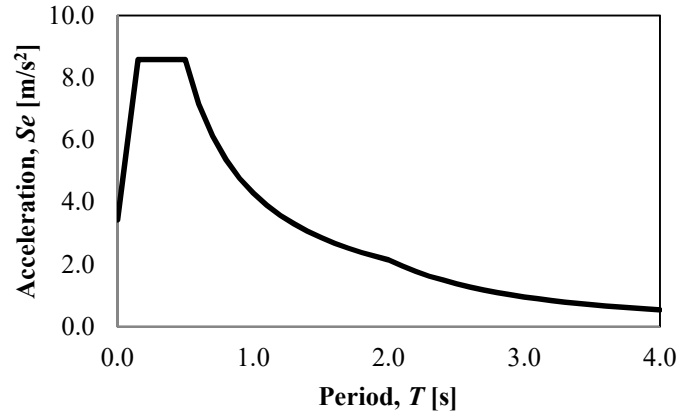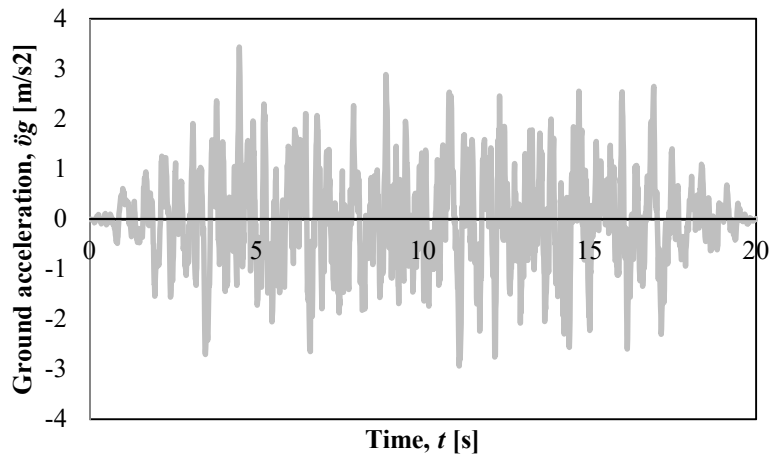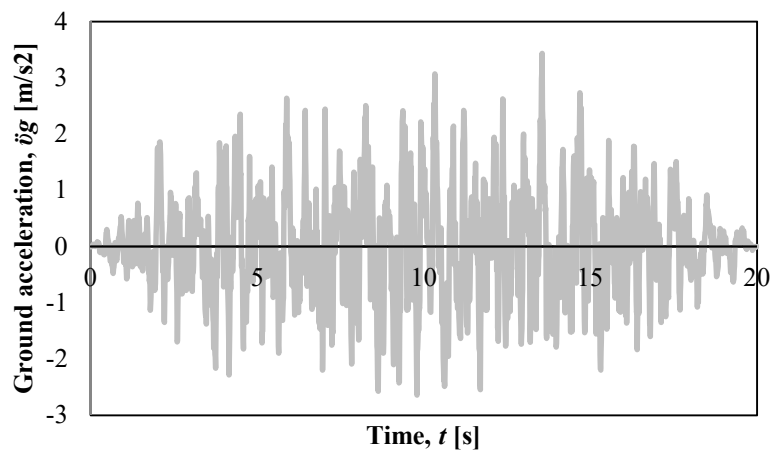
FIGURE 20: Elastic response spectrum for Famagusta based on a damping ratio of 5% and a ground type "D".

(a)

(b)

FIGURE 21: Unscaled time-history of accelerations with a PGA of 3.4 m/s^2, applied in the (a) X and (b) Y directions.

6.2.1 Analysis tools and parameters

To perform the analysis, additionally to the properties of Table 2, the damping matrix c of the structural system is simulated according to Rayleigh viscous damping. This is a procedure for constructing a classical damping matrix based on a linear combination of the mass m and stiffness k matrices, as of Equation 7 [Chopra, 2007]. The coefficients a_0 and a_1, which are inputs of the numerical model, are determined based on Equations 8 and 9, respectively. Here, ω_i and ω_j are the angular frequencies of modes i and j that are assumed to have the same damping ratio ξ.

$$c = a_0 m + a_1 k \tag{7}$$

$$a_0 = \xi \frac{2\omega_i \omega_j}{\omega_i + \omega_j} \tag{8}$$

$$a_1 = \xi \frac{2}{\omega_i + \omega_j} \tag{9}$$

Modes 1 and 2 were selected as the ith and jth modes, respectively, with angular frequencies equal to $\omega_1 = 35.9$ rad/s and $\omega_2 = 56.4$ rad/s. Chopra [2007] states that the experimental results of damping estimation based on low-amplitude forced vibration tests are usually disregarded because damping ratios determined from small structural motions are not representative of the larger damping expected at higher amplitudes of motions. Therefore, a damping ratio ξ of 3% was adopted for the selected modes, resulting in $a_0 = 1.3166$ and $a_1 = 0.0006$.

Concerning the time-stepping procedure needed for solving the equation of motion, the implicit Hilber-Hughes-Taylor (HHT) time-integration method was applied [DIANA FEA BV, 2018]. Masonry buildings have distributed cracking around the structure, featuring opening, closing and reopening of cracks due to the low masonry tensile strength. The quasi-brittle masonry behavior in tension introduces numerical noise due to the fast transition from a linear-elastic state to a fully cracked condition involving almost zero stiffness. These quasi-instantaneous changes in the displacement field tend to propagate high frequency spurious vibrations. The application of the HHT method, also known as the $\propto$-method, is thus of advantage as it eliminates the influence of non-realistic modes by introducing numerical damping of higher frequencies without degrading the degree of accuracy.

The HHT method is a generalization of the Newmark procedure. Its integration scheme is controlled by the parameters β and γ, expressed by Equations 10 and 11, respectively. For $\alpha = 0$ the procedure reduces to the Newmark method; and for $-1/3 \leq \alpha \leq 0$ the scheme is second-order accurate and unconditionally stable. Decreasing α means increasing the numerical damping, and the adopted damping is low for low-frequency modes and high for the high-frequencies modes. For the present analysis, following the recommendations of DIANA FEA BV [2018], α was set equal to -0.1.

$$\beta = \frac{1}{4}(1 - \alpha)^2 \tag{10}$$

$$\gamma = \frac{1}{2}(1 - 2\alpha) \tag{11}$$

Additionally, the time-step interval Δt was defined based on Equation 12, which is taken from [DIANA FEA BV, 2018] in order to account for the lowest period with relevance in the structural behavior T_i, with an error lower than 5%. Taking the period of mode 2 as the lowest period of importance ($T_2 = 0.1114$ s), a value of Δt equal to 0.00557 s is obtained.

$$\Delta t = \frac{1}{20} T_i \qquad (12)$$

Finally, concerning the iteration procedure, the linear-stiffness iteration method was applied along a convergence criterion based on the internal energy with a tolerance equal to 10^{-3}. Due to the high number of required steps, the cycles of loading-unloading and the robustness of the elastic-stiffness matrix, which is positive-definitive, the linear method is advantageous. This iteration method has, potentially, the slowest convergence with respect to other methods, such as the regular Newton-Raphson, but it costs the least time per iteration since the stiffness matrix needs to be set up only once.

6.2.2 Results

Figure 22 presents the envelopes of the hysteric behavior of the church in both directions and for the three earthquakes. Similarly to the pushover results, the horizontal displacement of the structure is based on the average displacement measured at the four top corners of the building. The maximum seismic coefficients (Earthquake 3) are 0.72 and 0.67 in the positive and negative X direction, respectively. In the Y direction, the maximum seismic coefficient is equal 0.53 either in both positive and negative directions. The results of the dynamic analysis allow to verify that the building reached its maximum load capacity in the Y direction, namely 0.53 g in transversal direction.

Figure 22 presents principal tensile strains (indicator of the damage) for the Earthquakes 1 and 2, in which is observed that the Church presents severe damage after the Earthquake 2 with generalized cracks over the entire structure. In the Earthquake 3, an extreme input was applied, aiming at reaching the full collapse of the structure. Thus, the Church presents very high deformations, which can be not realist and the structure collapse for a lower PGA and deformation. Thus, the principal tensile strains for the Earthquake 3 are not presented. It is noted that the damage pattern was obtained by scanning the maximum values of the tensile principal strain ε_1 through all the time-steps of the earthquake, because while performing time-history analyses, the generated cracks of the building pass through cycles of opening, closing and reopening along the different time-steps.

7. Discussion of the results

7.1 Numerical damage pattern vs. real damage of the Church

By comparing the numerical cracking pattern from Figure 18, with respect to the old and current real condition of the Armenian Church (Figures 5, 7 and 8), various damage features of the building can be justified and attributed to seismic actions. In particular, good accuracy of the damage location was obtained on the west and east sides of the building, namely the simulation of the current cracks around the west window and above the dome, as well as the damage at the top of the internal double-arch that leads to the

apse. Likewise, the past failure of the dome and of the section above, and the collapse of the west gable, can also be observed.
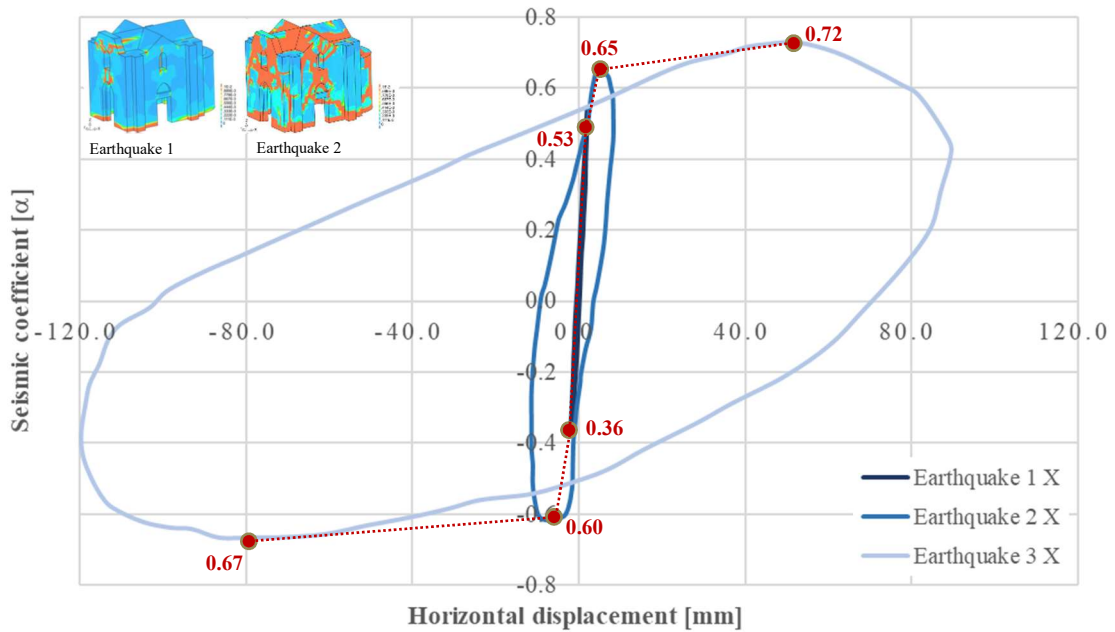
(a)
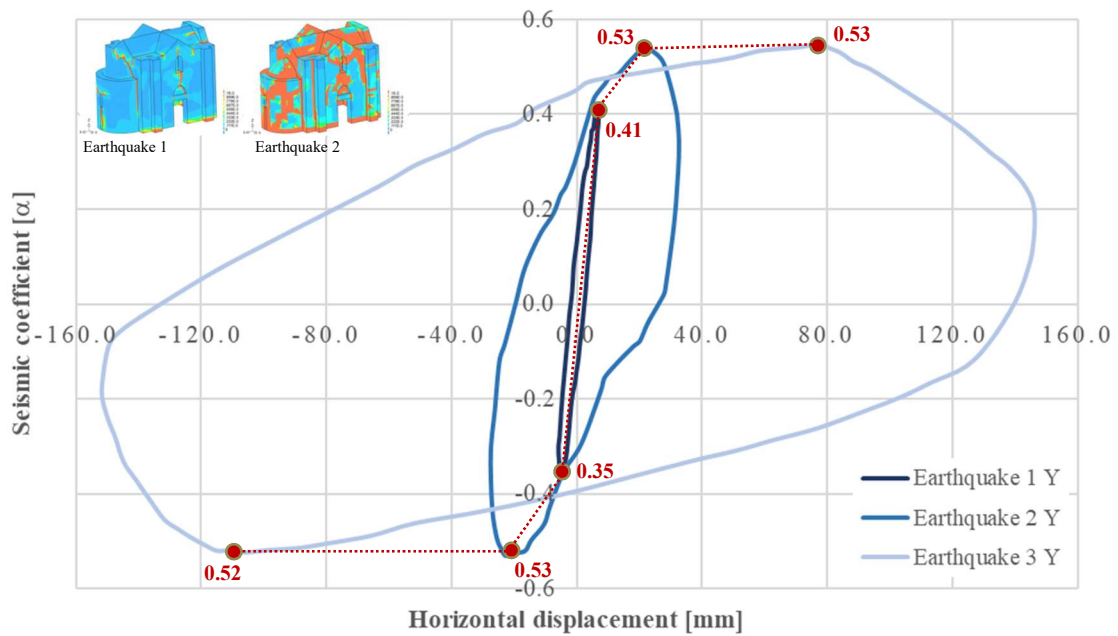
(b)

FIGURE 22: Envelopes of the relation between the horizontal displacement, measured at the top of the building, and the seismic coefficient: (a) in the longitudinal direction (X); (b) in transversal direction (Y).

PGA$_1$ = 3.4 m/s^2; PGA$_2$ = 6.8 m/s^2; PGA$_3$ = 13.6 m/s^2.

The red line represents the equivalent capacity curve obtained from the dynamic analysis, based on the maximum force.

In the Y direction, the structure presents high deformations for the Earthquake 3 and reached its load capacity for the Earthquake 2, indicating that the structure can collapse for a PGA lower than 13.6 m/s^2. Thus, the damage obtained for the Earthquake 3 can be not realist and it is not presented.

23

The cracks around the west window are also consistent with the information provided by the Damage Abacus [NIKER, 2010], which is an inventory that compiles typical seismic failure mechanisms of cultural heritage. According to this inventory, this crack pattern, commonly found in churches, can lead to an in-plane shear failure mechanism of the masonry structure causing either the failure of the whole façade or the localized failure of the top section of the window, as shown in Figure 23, a and b, respectively. In this case, the localized failure of the top of window can be related to the historical damage of the Church observed in Figure 5.

Concerning the longitudinal north and south walls, the current cracks between the openings can also be justified, as well as the historical partial collapse of the north entrance.

Finally, regarding the resulted numerical damage at the base of the structure, at present, the bottom part of the Church is highly affected by factors such as vegetation, material loss and deteriorated stone; therefore, it is difficult to ascertain which damage is consequence of past seismic actions and which is not.
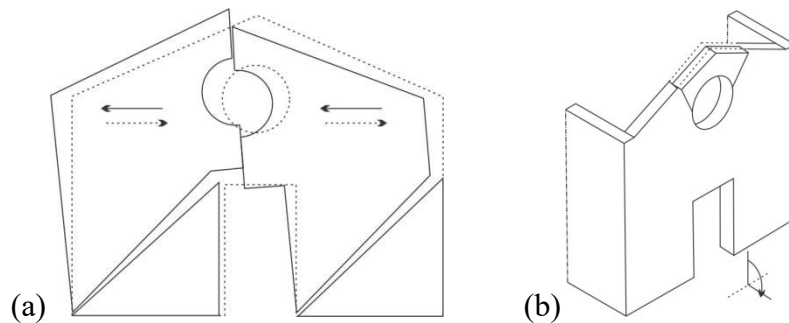

(a)   (b)

FIGURE 23: Typical seismic failure mechanisms of churches according to the Damage Abacus [NIKER, 2010]. In-plane shear failure mechanism of (a) the whole façade or (b) of the top section of the window.

7.2 Static vs. dynamic safety assessment

Comparing the results of the mass-proportional pushover and time-history analysis, several differences can be observed. Figure 24 demonstrates that the Earthquake 3 is associated to an extreme input, which was used mainly to reach the maximum load capacity and the full collapse of the building. Thus, the Church presents very high deformations for this earthquake and significant different from the results obtained from the pushover analyses (Figure 17), indicating that they can be unrealistic and the structure can collapse for a lower PGA (< 13.6 m/s^2). Besides the deformation, the maximum seismic coefficient obtained from the pushover analysis in the most vulnerable direction (Y direction) (0.25) is significantly lower than the capacity obtained from the dynamic analysis (0.53) (difference of about 50%). These differences can be attributed to the fact that: (a) the pushover analysis was only able to simulate the local failure of some elements of the Church, while the time-history analysis captured the global structural collapse; (b) the pushover analysis does not include the contribution of the higher modes; and (c) the pushover analysis was developed mainly for regular structures (in-elevation and in-plan) and with rigid diaphragms. It is noted that the pushover analysis with load pattern proportional to the first mode provides an even lower capacity (0.20 g). However, the maximum seismic coefficient obtained from the pushover analysis (0.74 and 0.67 in the positive and negative direction, respectively) and the dynamic analysis (0.72 and 0.67 in

the positive and negative direction, respectively) in the longitudinal direction of the Church is similar.

Despite the variations that the pushover and time-history results indicate, the structural analysis of the Armenian Church with time-history analysis points out that the structure presents an acceptable safety level in terms of both gravity and seismic loading, for ultimate limit states.

7.3 Present and future of the Armenian Church

Overall, it is worth noting the general good present state of the Armenian Church in comparison to other Famagusta buildings. While many Famagusta monuments are in a ruined condition, with only parts of the structure still standing, the Armenian Church is today characterized by less critical but not negligible issues. This situation can be attributed to the simplicity in the geometry of the building. The Armenian Church is a very sturdy structure, distinguished by thick walls and a moderate height, which are aspects that improve its structural behavior, preventing local damages and decreasing torsional effects in the event of an earthquake. In other words, there seems to be enough time to define an adequate intervention plan.

Future conservation works on the Armenian Church should address the damage discussed in Section 2. In particular, repair of the structure should include filling cracks, treating deteriorated stone, stabilizing loose stone units and replacing material loss. Furthermore, considering the importance of the fresco paintings at the interior, the vault should be treated to prevent water infiltration, windows should be protected and cracks would need to be monitored to characterize their activity. On the long-term, in order to fully revitalize the ancient appearance of the building, a detailed study of the north portal (currently blocked with brick masonry) should be carried out with the aim of re-opening the entrance.

8. Conclusions

This work presents the results of the in-situ investigation and structural analysis of the Medieval Armenian Church in Famagusta. An extensive characterization of the condition of the building was done, including historical photographic survey, damage mapping and application of non-destructive tests, namely sonic testing and dynamic identification. Moreover, non-linear structural analyses were performed, using a tridimensional finite element model, by means of pushover and time-history analysis. These analyses indicate that the pushover method must be used carefully for historic structures, as it predicted an excessively lower load capacity for the structure considered.

The structural analysis of the Armenian Church indicated, in general, that the building has a considerable safety level against vertical and horizontal loading, which is attributed to the regularity of the structure, its moderate height and sturdiness.

Regarding the static pushover method, the application of a mass-proportional loading pattern helped understanding past and current damage features of the building. Most of these features were attributed to seismic actions; particularly, the cracking around the corners of the openings, which is a typical damage characteristic of masonry buildings. Also, local failure of some structural elements, such as the collapse of the west gable and of the top of the dome, were simulated and are consistent with the historical damage of the building.

The influence of the mass distribution of the Church in its structural behavior was also studied. This was achieved by comparing the results of the mass-proportional pushover loading pattern with respect to a loading pattern proportional to the first mode of vibration. Two approximations of the Eurocode 8 procedure were used: one where loads were proportional to modal displacements only, and other where, in addition, the mass of the building was defined using a lumped mass matrix. The first procedure gave poor results while the second one presented a better approximation with respect to the mass-proportional approach. The maximum seismic coefficient was reduced about 20%, with respect to mass-proportional loading.

Concerning the time-history analysis, the results allowed to conclude that the structure reaches its maximum seismic coefficient in the transversal (0.53), and most vulnerable direction, for Earthquake 2 with PGA equal to 6.8 m/s^2, which is about the double of the maximum seismic coefficient obtained from the pushover analysis (0.25). This difference between the pushover and time-history results is explained by the fact that the first one was only able to estimate localized failures of the structure and that static analysis fail to consider adequately the dynamic effects. In the longitudinal direction, the pushover analysis with load patter proportional to the mass and the dynamic analysis presented similar maximum seismic coefficients.

Acknowledgements

References

ARTeMIS [2018] *Ambient Response Testing and Modal Identification Software.* Developed by Structural Vibration Solutions A/S, Aalborg East, Denmark.

Binda, L.; Saisi, A. and Tiraboschi, C. [2001] "Application of sonic tests to the diagnosis of damaged and repaired structures," Non Destructive Testing and Evaluation Int. 34(2), pp. 123-138.

Chiaia B.; Van Mier, J.G.M. and Vervuurt, A. [1998] "Crack growth mechanisms in four different concretes: microscopic observations and fractal analysis", Cement and Concrete Research, 28 (2), pp. 103-114.

Chopra, A. K. [2007] Dynamic of Structures – Theory and Applications to Earthquake Engineering. Third Edition, Prentice Hall, Inc., New Jersey, USA.

CYS EN 1998-1:2004 [2010] National Annex to Eurocode 8: Design of structures for earthquake resistance – Part 1: General rules, seismic actions and rules for buildings.

DIANA FEA BV [2018] *DIANA Finite Element Analysis User's Manual.* Release 10.2. Delft, the Netherlands.

EN 1998-1 [2004] Eurocode 8: Design of structures for earthquake resistance – Part 1: General rules, seismic actions and rules for buildings.

Endo, Y., Pelà, L., Roca, P. [2017] "Review of different pushover analysis methods applied to masonry buildings and comparison with nonlinear dynamic," Journal of Earthquake Engineering, 21, pp. 1234-1255.

Enlart, C. [1899] Gothic art and Renaissance in Cyprus (Translated by David Hunt. Reissued 1987). London: Trigraph & the Leventis Foundation.

Gelfi, P. [2006] *SIMQKE_GR – Artificial earthquakes compatible with response spectra*, University of Brescia, Italy.

Langdale, A. and Walsh, M. J. K. [2009] "The architecture, conservation history and future of the Armenian Church of Famagusta, Cyprus," in CHRONOS 19: Revue d'Histoire de l'Université de Balamand, pp. 7-40.

Lourenço, P. B. [2010] "Recent advances in masonry modeling: micromodelling and homogenization," in Computational and Experimental Methods in Structures – Vol 3, Multiscale Modeling in Solid Mechanics, eds. Galvanetto U. and Ferri Aliabadi M.H., pp. 251-294.

Lourenço, P. B.; Trujillo, A.; Mendes, N. and Ramos, L. F. [2012] "Seismic performance of the St. George of the Latins church: Lessons learned from studying masonry units," Engineering Structures 40, pp. 501-518.

Lydon, F. D. and Balendran, R. V. [1986] "Some observations on elastic properties of plain concrete," Cement and Concrete Research 16(3).

Marques, R., Pereira, J.M., Lourenço, P.B., Parker, W., Uno, M. [2013] "Study of the seismic behavior of the "Old Municipal Chambers" building in Christchurch, New Zealand," Journal of Earthquake Engineering, 17(3), p. 350-377.

Mendes N. [2012] "Seismic assessment of ancient masonry buildings: Shaking table tests and numerical analysis", PhD Thesis, University of Minho, Portugal.

Mendes, N. and Lourenço, P. B. [2010] "Seismic assessment of masonry "Gaioleiro" buildings in Lisbon, Portugal", Journal of Earthquake Engineering, 14, pp. 80-101.

Milani, G., Valente, M., [2019] "Damage survey, simplified assessment, and advanced seismic analyses of two masonry churches after the 2012 Emilia earthquake", International Journal of Architectural Heritage, in press.

NIKER, New Integrated Knowledge based approaches to the protection of cultural heritage from Earthquake-induced Risk [2010]. *Damage Abacus – Inventory of earthquake-induced failure mechanisms related to construction types, structural elements and materials.* Available from http://www.niker.eu/downloads/

Peña, F., Lourenço, P.B., Mendes, N., Oliveira, D.V. [2010] "Numerical models for the seismic assessment of an old masonry tower, Engineering Structures," 32(5), pp. 1466-1478.

Roca, P., Cervera, M., Pelà, L., Clemente, R., Chiumenti, M. [2013] "Continuum FE models for the analysis of Mallorca Cathedral", Engineering Structures, 46, pp. 653-670.

Safkan, I. [2012] "Comparison of Eurocode 8 and Turkish Earthquake Code 2007 for Residential RC Buildings in Cyprus", in Proc. 15th World Conference on Earthquake Engineering, paper 2990.

Seismosoft [2018] *SeismoSignal – A computer program for signal processing of strong-motion data.*

Unit of Environmental Studies [2004] *Cyprus geological heritage educational tool. The seismicity of Cyprus.* Research and Development Center. Available from: http://www.cyprusgeology.org/english/index.htm.

Vasconcelos G. [2005] "Experimental investigations on the mechanics of stone masonry: Characterization of granites and behavior of ancient masonry shear walls", PhD Thesis, University of Minho, Portugal.

Votsis, R.A., Kyriakides, N. Tantele, E.A., Chrysostomou, C.Z. [2015] "Effect of Damage on the Dynamic Characteristics of St. Nicholas Cathedral in CYPRUS" in Seismic Assessment, Behavior and Retrofit of Heritage Buildings and Monuments, eds. Psycharis I. et al., pp. 281-295.

World Monuments Watch [2008] *2008 List of 100 Most Endangered Sites.* Available from: https://www.wmf.org/sites/default/files/press_releases/pdfs/2008%20Watch%20List.pdf.